AGU PUBLICATIONS

JGR

Journal of Geophysical Research: Space Physics

RESEARCH ARTICLE

10.1002/2013JA019336

Key Points:
- Quiet time convection of plasma sheet ions is simulated
- Gradient drift is assessed as a cooling mechanism for hot component plasma
- Gradient drift may explain observed cooling of dawn but not dusk flank plasma

Correspondence to:
C. Lemon,
colby@aero.org

Citation:
Mata, W. J., C. Lemon, C.-P. Wang, and L. R. Lyons (2014), Density and temperature evolution of the plasma sheet during a simulated interval of northward interplanetary magnetic field, *J. Geophys. Res. Space Physics*, *119*, 4607–4620, doi:10.1002/2013JA019336.

Received 16 AUG 2013
Accepted 24 MAY 2014
Accepted article online 29 MAY 2014
Published online 19 JUN 2014

Density and temperature evolution of the plasma sheet during a simulated interval of northward interplanetary magnetic field

Wendy J. Mata[1], Colby Lemon[2], Chih-Ping Wang[1], and Larry R. Lyons[1]

[1]Department of Atmospheric and Oceanic Sciences, University of California, Los Angeles, California, USA, [2]Space Sciences Department, The Aerospace Corporation, El Segundo, California, USA

Abstract We investigate the evolution of the hot component of plasma sheet ions during an extended interval of northward interplanetary magnetic field and assess whether transport can explain the observed cooling of the hot component ions reported by Wing et al. (2005). Our approach is to trace the guiding center particle drift of protons in a magnetic field from the Tsyganenko 2001 (T01) model and in an electric field from the Weimer 2000 model. We then map the phase space distributions to realistic source distributions based on Time History of Events and Macroscale Interactions during Substorms observations. Our simulation results show that magnetic drift is not a significant cooling mechanism for the hot component ions of the plasma sheet on the duskside of the magnetopause, but gradient drift does cool the hot component plasma on the dawnside of the magnetopause.

1. Introduction

1.1. The Plasma Sheet

The plasma sheet is about 6 R_E thick and consists of hot particles in the magnetotail that extends into and around the Earth's dipole [*Borovsky et al.*, 1998] and stretches tens of R_E down the Earth's magnetotail. The plasma sheet lies on closed but extended field lines with flow velocities much smaller than the ion thermal velocity [*Kivelson and Russell*, 1995]. Number densities in the plasma sheet are typically 0.1–1 cm^{-3}, and the average ion temperature (a few keV) is about 7 times the electron temperature [*Baumjohann et al.*, 1989; *Wang et al.*, 2012]. The plasma sheet gets denser and hotter with decreasing distance to the Earth [*Huang and Frank*, 1994; *Borovsky et al.*, 1998; *Wing and Newell*, 1998].

The solar wind and the polar ionosphere both contribute to the plasma sheet particle population, which consists mainly of hydrogen ions and their associated electrons. Currently, the details of the particle entry processes and of the loss processes are not fully understood [*Prölss*, 2004].

The solar wind transfers energy to the magnetosphere. Some of this energy is lost via auroral particle precipitation, some of it is lost via auroral ionospheric currents, some of the energy shows up in the ring current, and some of the energy is lost via plasmoids [*Kamide and Slavin*, 1986; *Weiss et al.*, 1992]. Since the auroral particles and currents originate in the plasma sheet [*Feldstein and Galperin*, 1985; *Mauk and Meng*, 1991] and since the source of the ring current particles is the plasma sheet [*Harel et al.*, 1981; *Jordanova et al.*, 1994], and since plasmoids originate from plasma sheet material [*Hones*, 1984; *Moldwin and Hughes*, 1992], the plasma sheet plays a significant role in the transfer of energy from the solar wind to the Earth.

1.2. The Plasma Sheet During Northward Interplanetary Magnetic Field

During northward interplanetary magnetic field (NIMF) intervals the plasma sheet is colder and denser than during southward interplanetary magnetic field (SIMF) intervals [e.g., *Terasawa et al.*, 1997; *Wing and Newell*, 2002; *Wing et al.*, 2005; *Øieroset et al.*, 2005]. This is generally understood to be due to the entry of cold magnetosheath plasma into the magnetosphere via the low-latitude boundary layer region, leading to the formation of what is referred to as the cold dense plasma sheet [*Fujimoto et al.*, 1998, 2000]. The NIMF or quiet time plasma sheet plays an important preconditioning role in the development of geomagnetic activity during SIMF intervals, since the more abundant cold plasma that builds up during NIMF periods can provide more source particles for the inner magnetosphere than under SIMF periods and thus result in stronger geomagnetic disturbances after a sudden SIMF turning [*Thomsen et al.*, 2003; *Lavraud et al.*, 2006; *Borovsky and Steinberg*, 2006]. For example, the simulation results from *Lavraud and Jordanova* [2007] in

which kinetic ring current simulations were made with different plasma boundary conditions show that the proton ring current energy is larger for the coldest and densest plasma.

During prolonged NIMF intervals, the plasma sheet density increases by a factor of approximately 3, and the ion temperature decreases from a few keV to 1 keV or less [*Terasawa et al.*, 1997; *Øieroset et al.*, 2005]. Furthermore, these studies make clear that a very brief northward turning is not enough to dramatically cool and densify the plasma sheet and that extended intervals (several hours or more) are required before significant quantities of cold dense plasma can begin to permeate the plasma sheet.

1.3. Two-Component Distribution of Ions During NIMF

Spence and Kivelson [1993] modeled the quiet time earthward transport of magnetotail plasma from a distant tail source, including $E \times B$ and gradient/curvature drift, and found that gradient/curvature drift drives sufficient duskward transport that pressure in the near-tail dawn flank would be too weak unless a dawnside low-latitude boundary layer source of cold plasma is also included in the model. Their model included a very simple convection electric field that did not include full circulation of plasma (including tailward flow along the flanks) but still was suggestive of the necessity of modeling the plasma sheet ions using two-component distributions. *Wang et al.* [2001] modeled quiet time earthward transport with a more realistic electric and magnetic field (though still not including the full circulation) and came to a very similar conclusion.

Observations have shown a two-component distribution of ions in the plasma sheet consisting of a colder magnetosheath-like component that is dominant near the flanks and a hotter component that is dominant near midnight [*Wing et al.*, 2005; *Wang et al.*, 2007]. The ions can be separated into a two-component distribution [e.g., *Wing et al.*, 2005] when the hot component and cold component temperatures are significantly different from each other. The typical temperature of the cold component is $\sim$ 345–517 eV (~ 4–6×10^6 K), which is also the typical temperature of the magnetosheath ions [e.g., *Fujimoto et al.*, 1998], and the typical temperature of the hot component is 4.3 keV ($\sim 5 \times 10^7 K$), consistent with the nominal plasma sheet population [e.g., *Lennartsson and Shelley*, 1986; *Baumjohann et al.*, 1989; *Huang and Frank*, 1994; *Fujimoto et al.*, 1998]. The cold component is likely to have recently entered from the magnetosheath while the hot component is likely leftover plasma that entered from the mantle during SIMF [*Wing et al.*, 2005].

Wing et al. [2005] fit a two-component distribution and obtained density, temperature, and pressure from observations made at low altitudes by Defense Meteorological Satellite Program (DMSP) satellites. By using a fitted spectrum, they included energies from outside the DMSP detector's range (32 eV–30 keV). The results were mapped to the magnetotail using the T89 magnetic field model [*Tsyganenko*, 1989]. Their results show that the cold component densities peak along the flanks and increase in time the longer the IMF is northward. Furthermore, there is a slight temperature asymmetry between the dask and dusk flank, with the cold component ions being hotter on the dawn flank by about 100 eV [*Wing et al.*, 2005]. Figure 1 (reproduced from *Wing et al.* [2005]) shows how the average density and the average temperature of the cold and hot component ions of the two-component population evolve along both flanks. The dashed line is for $y > 15\ R_E$ and the solid line is for $y < -15\ R_E$ for x between $-15\ R_E$ and $-30\ R_E$. Figure 1a shows that along both flanks, the cold component density increases the longer the interplanetary magnetic field (IMF) has been northward, while the temperature of the cold component remains relatively constant. The constant temperature is consistent with a magnetosheath source for the cold component because the magnetosheath ion temperature is not expected to change with the duration of NIMF. However, as noted above, the average temperature does show a dawn-dusk asymmetry suggesting that the dawnside magnetosheath ions may be heated by about 100 eV.

On the other hand, as seen in Figure 1, the hot component temperature decreases the longer the IMF has been northward. The cause for this cooling is not immediately clear; however, *Wing et al.* [2005] suggest various hypotheses including the following: wave interactions between the hot and cold components that cool the hot component and heat the cold component, a preferential loss of hotter ions through ionospheric precipitation, and gradient and curvature drift cooling of the hot component. In this paper, we evaluate the extent to which gradient drift can account for the cooling of the hot component ions.

2. Methods

2.1. Guiding Center Drift

To test whether or not gradient drift can explain the cooling of the hot component ions of the plasma sheet during an extended interval of continuous NIMF, we trace the guiding center particle drift of protons in

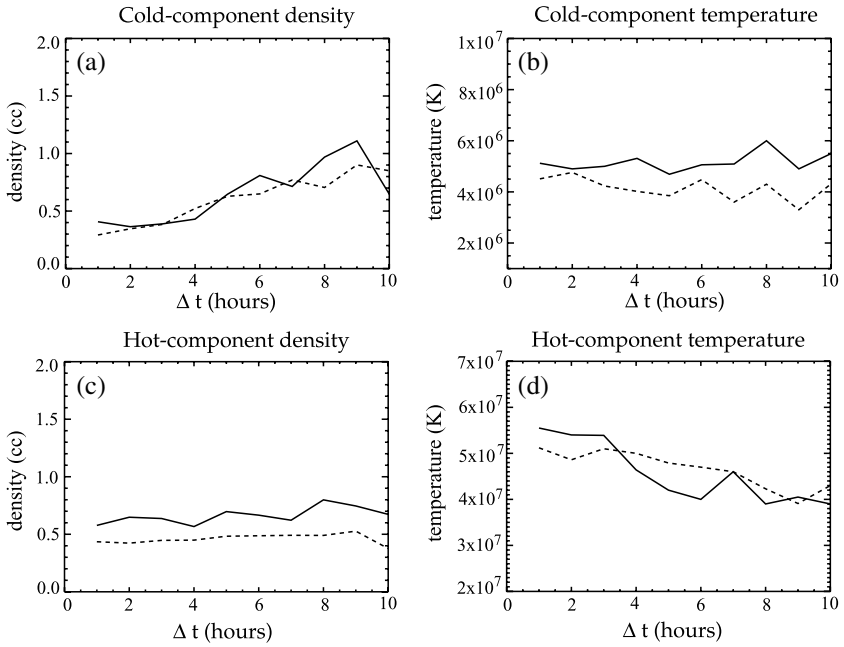

Figure 1. Observed evolution of the cold and hot components of the two-component Maxwellian distribution along the dawn flank (dashed line) and along the dusk flank (solid line) inferred from DMSP observations. Figure reprinted from *Wing et al.* [2005].

the T01 magnetic field and in the Weimer 2000 electric potential and then map the resulting phase space distributions to realistic source distributions based on observations. We follow the guiding center drift of approximately 23,275 protons with 90° pitch angles and energies ranging from 32 eV to 30 keV. We note that even though we only simulate hot component ions, this does not mean that we only simulate "hot ions". There is significant overlap in the energy spectrum of cold component and hot component ions. We use a comprehensive energy range to fully characterize the drift of hot component ions at both ends of the energy spectrum. By considering 90° particles, we do not need to be concerned with curvature drift or with breaking of adiabatic motion by the field line curvature [*Young et al.*, 2008]. Also, because the tail current is relatively weak during a NIMF interval, the T01 magnetic field has only a mild spatial gradient over the scale of a particle gyroradius. The trajectories of these protons are traced inside a modeling region from $-50 < X < -10\ R_E$ and $-24 < Y < 24\ R_E$ in an effort to investigate the cooling of the hot component ions during an extended interval of continuous NIMF.

The particle trajectories are obtained by solving the Lorentz force equation under the assumption that the first adiabatic invariant is conserved. A locally determined adaptive step size, which uses the instantaneous guiding center drift force terms, is used to set Δt at each time step. The following NIMF upstream solar wind parameters were used to drive the electric and magnetic field models in the Lorentz force particle tracer: $n_{sw} = 4.8\ \mathrm{cm}^{-3}$, $v_{sw} = 500$ km/s, IMF $B_y = 0$ nT, and IMF $B_z = 4$ nT. For our energy range (32 eV–30 keV) the guiding center drift is justified because the tail current is relatively weak during NIMF, leading to a relatively large radius of curvature for the field lines, and therefore relatively weak pitch angle scattering. Nevertheless, field line curvature is sharper than in the inner magnetosphere, and we expect modest pitch angle scattering should be occurring in the plasma sheet even during intervals of NIMF. We believe that neither the assumption of zero pitch angle scattering nor that of strong pitch angle scattering is justified. Our choice of simulating 90° particles is therefore largely for convenience, since it allows us to devote our computational resources to simulating more particle locations in the plasma sheet, and more energies, rather than simulating multiple pitch angles.

2.2. Magnetic and Electric Field Models

The T01 model is an empirical magnetic field model of the Earth's inner and near magnetosphere, for different interplanetary conditions and for different levels of the ground disturbance. The T01 magnetic field is represented in modular fashion in which the external part of the total field is represented as a sum of

contributions from the field of the Chapman-Ferraro current, the ring current, the cross-tail current sheet, the large-scale field-aligned currents, and the contribution resulting from the partial penetration of the IMF inside the model magnetosphere [*Tsyganenko*, 2002a]. The modeling database is mostly from space magnetometer data including 5 min averaged magnetic field data taken in a wide range of altitudes and latitudes by the International Solar Terrestrial Physics Spacecrafts Polar and Geotail as well as by earlier missions: ISEE 2, Active Magnetospheric Particle Tracer Explorer (AMPTE)/CCE, AMPTE/Ion Release Module, CRRES, and DE1. The space magnetometer data are complemented by concurrent solar wind and ground-based observations [*Tsyganenko*, 2002b].

The Weimer electric field model is a model of ionospheric electric potential/convection patterns, based on spherical harmonic coefficients derived with a least error fit with satellite measurements of electric potential. The Weimer model produces potentials for any level of IMF, solar wind velocity, number density, and dipole tilt angle, as well as an optional value for the *AL* index [*Weimer*, 2001]. The database consists of electric fields measured on the Dynamics Explorer-2 satellite [*Maynard et al.*, 1981] in combination with solar wind/IMF measurements from the IMP 8 and ISEE 3 satellites.

2.3. Study Limitations

Some of the limitations we confront include the following: (1) the T01 magnetic field model is fit with data earthward of $-15\ R_E$, but our simulations require magnetic field data beyond $-15\ R_E$, (2) we assume steady IMF and solar wind conditions, which is idealistic, and (3) our simulations do not include waves, which could lead to pitch angle scattering and/or diffusive transport, and so by ignoring these processes, we do not fully capture all of the possible plasma transport mechanisms.

Although the T01 data are earthward of $-15\ R_E$, we use this model in the plasma sheet because it gives more qualitatively reasonable results as compared to other models. For example, there is an inherent artificial B_z minimum in the T96 model near the center of the plasma sheet that causes the higher energy protons to drift around in circles. We increased both the IMF B_z and the *Dst* in the T96 model in order to transfer some magnetic flux from the inner magnetosphere to the tail, but the high-energy particles continued to drift around in circles. These shortcomings can be remedied by using alternative electric and magnetic field models from (e.g.) the Rice Convection Model-Equilibrium (RCM-E). However, the RCM boundary conditions would not allow us to model plasma circulation, only the influx and efflux of plasma on field lines equatorward of the polar cap. In addition, one of the main advantages of using the T01 magnetic field model and the Weimer electric potential model is that they are relatively simple, and we can easily control these fields and experiment with different scenarios as opposed to using MHD models in which the fields are determined by a mixture of model physics and numerics that are more difficult to control.

2.4. Model Setup

A rectangular array of points is divided spatially into 19 bins in the x direction from $x = -10\ R_E$ to $-50\ R_E$ with $2.2\ R_E$ separation and 49 bins in the y direction from $y = -24\ R_E$ to $24\ R_E$ with $1\ R_E$ separation. At each point, we simulate, 25 proton energies ranging logarithmically from 32 eV to 30 keV and with 90° pitch angles.

We selected times $t = 1, 2, 3, \ldots, 10$ h and traced protons backward in time to either $t = 0$ or to a boundary, such as the magnetopause or the tail boundary of the simulation, if a boundary is reached at a time $t > 0$. The tail boundary is taken to be at $x = -50\ R_E$. Figure 2 shows two representative trajectories traced backward in time from the point $(-34.4, 10)$ overlaid on the Weimer electric potential contours. The blue curve is a 32 eV proton and the black curve is a 30 keV proton. As expected, the low-energy proton (blue curve) closely follows the equipotential contours while the highest-energy proton (black curve) deviates significantly due to gradient drift. By tracing backward in time, we are able to fill the domain of interest and obtain the source of protons that intersect that location in phase space. We then obtain the appropriate phase space density by specifying initial and boundary particle conditions.

We have established the initial and boundary particle conditions based on statistical Time History of Events and Macroscale Interactions during Substorms (THEMIS) observations during periods when the IMF had been northward or southward for at least 4 h. We used measurements from three of the five THEMIS spacecraft (TH-B, TH-C, and TH-D) from 23 March 2007 to 31 August 2011. The THEMIS spacecraft are in low-inclination, near-equatorial orbits. TH-D covers regions inside r $\sim 12\ R_E$, while TH-B and TH-C cover regions inside $r \sim 70\ R_E$ [*Wang et al.*, 2012]. There are very few THEMIS observations between

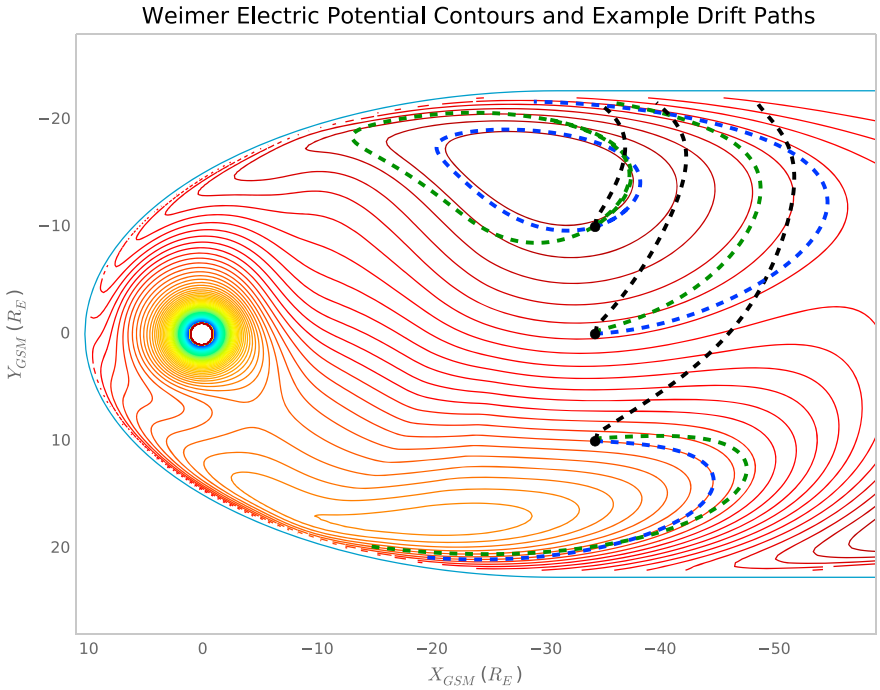

Figure 2. Equipotentials (solid lines) from the Weimer model have been mapped along T01 magnetic field lines to the equatorial plane. Inputs used to drive the field models are $n_{sw} = 4.8$ cm^{-3}, $v_{sw} = 500$ km/s, IMF $B_y = 0$ nT, and IMF $B_z = 4$ nT. Example trajectories (dashed lines) are shown for protons of energy 32 eV (blue), 5.4 keV (green), and 30 keV (black). These trajectories map particles from the locations indicated by the three black points to their computed source locations.

$r \sim 30\,R_E$ and $\sim 40\,R_E$, and the results in this gap are filled by interpolation. THEMIS observations are fit to a two-component kappa distribution [*Wang et al.*, 2012] of the form

$$f_\kappa(W) = n\left(\frac{m}{2\pi\kappa W_0}\right)^{\frac{3}{2}} \frac{\Gamma(\kappa+1)}{\Gamma(\kappa-\frac{1}{2})}\left(1+\frac{W}{\kappa W_0}\right)^{-(\kappa+1)} \tag{1}$$

where n is density, m is mass, and W is kinetic energy [*Baumjohann and Treumann*, 1997]. W_0 is the peak of the energy distribution and can be related to the average thermal energy by

$$W_0 = k_B T\left(1-\frac{3}{2\kappa}\right) \tag{2}$$

Because this study addresses the evolution of the hot component ions, we do not use the cold component of the two-component distribution for any of our initial or boundary conditions. In addition, the hot component data have been smoothed using a Gaussian filter with $\sigma = 2.5\,R_E$ in order to remove some of the statistical fluctuations from the data binning. Figure 3 presents the data set used to provide our initial and boundary conditions. The peaks and troughs in the density and temperature observed in the region from $x \sim -30\,R_E$ to $\sim -40\,R_E$ are likely due to poor statistics in that region, and our Gaussian smoothing aims to minimize any simulation artifacts that might be caused by such statistical fluctuations.

The initial condition is applied to the protons that trace back to time zero without having encountered a model boundary. It is specified as the proton's phase space density at the source location inside the region $-10\,R_E < x < -50\,R_E$ and $|y| < 24\,R_E$ determined from SIMF THEMIS observations with $1\,R_E \times 1\,R_E$ spatial resolution. The plasma boundary condition is applied to the protons that trace to a boundary at times $t > 0$ and is obtained from NIMF THEMIS observations. In either case, the particle's energy at its source location is in general different from its energy at other locations, and the phase space mapping relates the particle's initial and final energies in order to apply the correct value for the phase space density.

Because the observed cooling of the hot component ions occurs over a period of many hours [*Wing et al.*, 2005], we do not begin the simulated interval of NIMF with a stretched magnetic field or an enhanced electric field. Our reasoning is that some intervals of NIMF begin with weakly stretched fields, while others begin

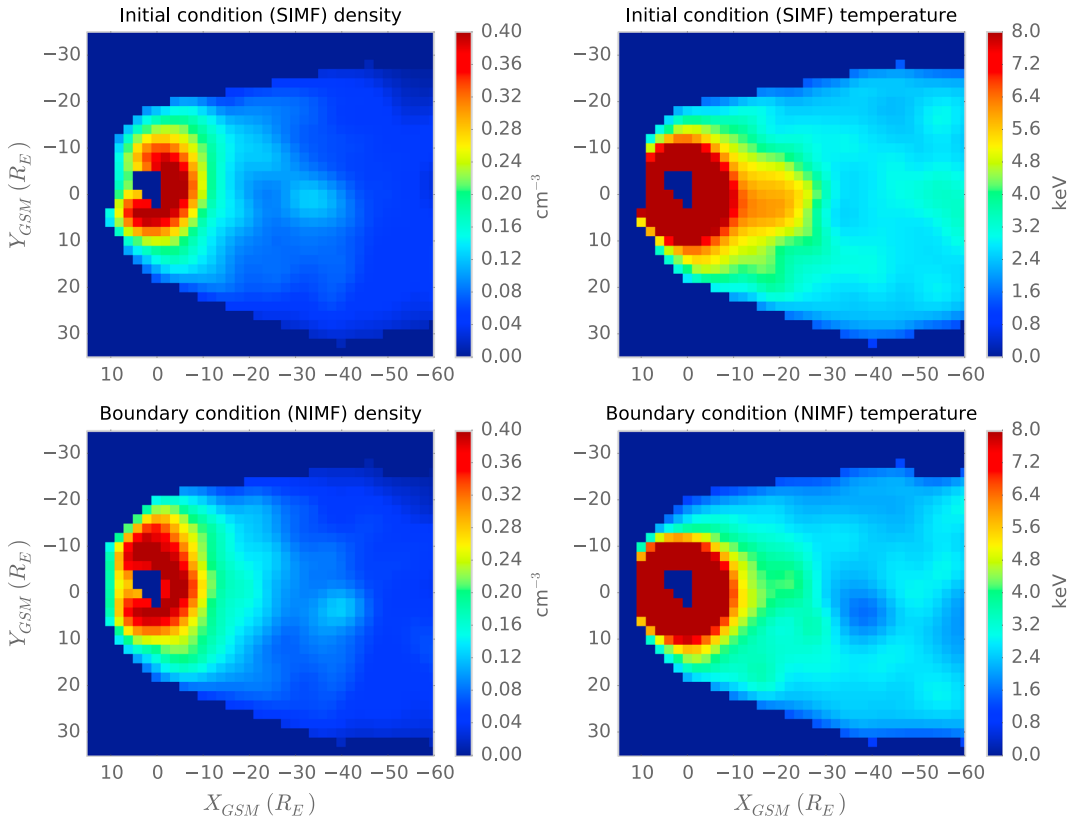

Figure 3. Density and temperature of the hot component plasma used to specify our initial and boundary conditions. (top) The initial condition is spatially-smoothed THEMIS data obtained during southward IMF intervals, while the (bottom) boundary condition is from THEMIS data obtained during northward IMF intervals.

with more strongly stretched fields and possibly a substorm expansion phase. Since we are interested in a long-term cooling mechanism, we specify a quiet time magnetic field that is constant throughout the simulation. In that sense, it might be more accurate to say that we simulate the first 10 h after the magnetosphere enters a quiet time state, rather than the first 10 h after a northward turning of the IMF. Our initial condition for the plasma phase space density is based on the assumption that the quiet time state is achieved relatively quickly after the northward turning, so that a plasma sheet consistent with SIMF conditions is a reasonable approximation for our initial condition.

2.5. Three Simulation Cases

We ran three separate simulation cases: (case 1) the initial condition is obtained from SIMF THEMIS observations and the boundary condition for phase space density is set to zero in order to show where the preexisting SIMF plasma is going in the absence of new plasma entry; (case 2) the initial condition for phase space density is set to zero and the boundary condition is obtained from NIMF THEMIS observations in order to show the entry of NIMF plasma; and (case 3) the initial condition is obtained from SIMF THEMIS observations and the boundary condition is obtained from NIMF THEMIS observations to simulate the mixing of new and preexisting hot component plasma. In case 1, by setting the boundary condition to zero, we effectively assume that the hot component ions do not enter during NIMF intervals. Assuming that there is no entry of any new particles (cold or hot component ions) during NIMF would be unrealistic since the source of the cold component ions, which we do not model in this paper, is believed to be of magnetosheath origin, and it is known that the cold component ions preferentially enter during NIMF intervals [*Wing et al.*, 2005]. The cold component density therefore increases during NIMF intervals (as seen in Figure 1). However, this study focuses only on the hot component ions and thus ignores any entry of cold component ions throughout the NIMF interval of the simulation. From the mapped phase space densities, the density and temperature evolution of the hot component ions in the region enclosed by $x = -10\,R_E$ to $-50\,R_E$ and

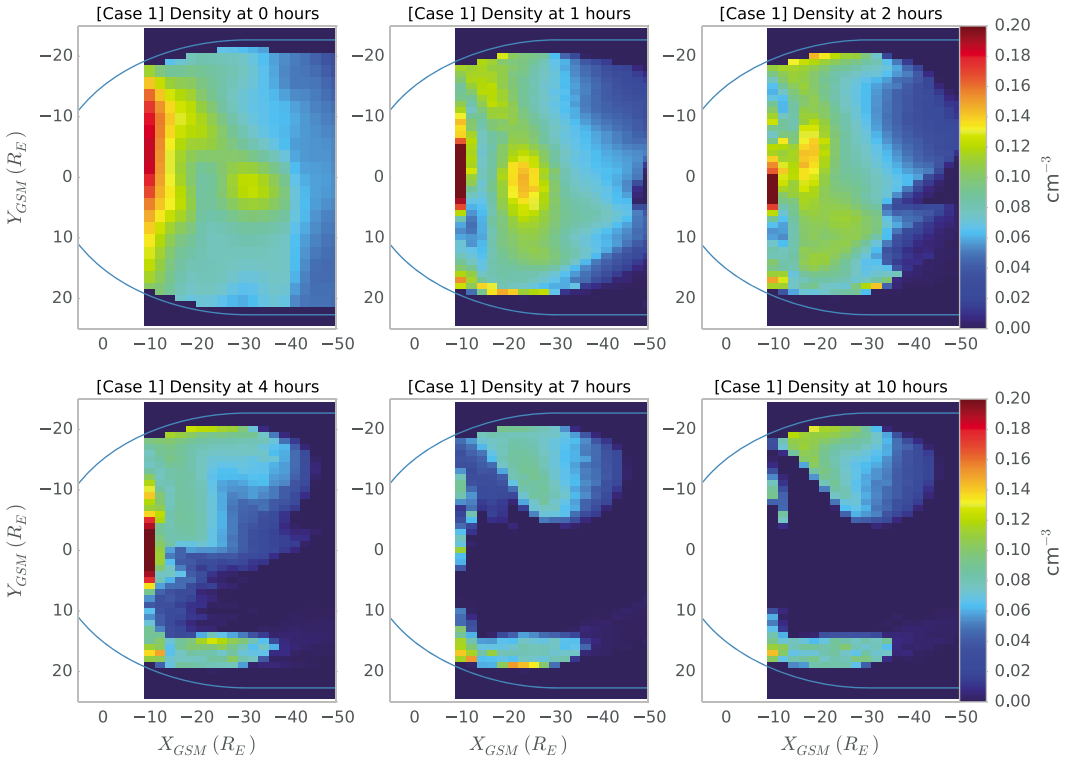

Figure 4. The hot component density from the Case 1 simulation is shown at times 0, 1, 2, 4, 7, and 10 h. The location of the magnetopause in the T01 magnetic field model is shown for reference.

$y = -24\,R_E$ to $24\,R_E$ is determined from moment calculations. Figure 3 shows the density and temperature THEMIS data set that is used to specify the initial and boundary conditions.

3. Results

3.1. Case 1

In case 1 we simulate what might occur if there were no new (hot component) plasma entry into the modeling region by setting the boundary phase space density to zero. Comparing the density evolution plots (Figure 4) with the temperature evolution plots (Figure 5), which at $t = 0$ are the same as Figure 3 (top), the regions that are bright red in the temperature plots correspond to regions where the density is seen to drop to near zero. Since we artificially prevent new plasma from entering the modeling region, these bright red regions represent areas where the coldest particles no longer have access, because they are carried away by $E \times B$ drift and are not replaced by new cold particles. However, residual hot particles still have access to these locations because they are drifting from elsewhere in the modeling region. Since high-energy particles are able to drift across equipotential contours, they have access to regions where there is an absence of low-energy plasma. As an example, we note that there is a shallow B_Z minimum on the dusk region of the tail flank around which the hottest protons drift on closed orbits. Once the low- and medium-energy plasma has drifted out of this region, only these energetic protons remain, and we are left with a very hot and very tenuous plasma. Earthward of this region of hot tenuous plasma is a region of relatively cold and dense plasma where the opposite is true: colder plasma moves on closed drift orbits following equipotentials (see Figure 2), while the hottest plasma is not trapped on these orbits. In this simulation run, we observe that the dawn flank which we define as $y < -15\,R_E$ cools by about 20% from $t = 0$ to $t = 1$ h when averaged over $x = -15\,R_E$ to $-50\,R_E$, and the dusk flank which we define as $y > 15\,R_E$ warms up by about 9% from $t = 0$ to $t = 3$ h when averaged over $x = -15\,R_E$ to $-50\,R_E$. After 1 h, the temperature on the dawn flank remains fairly constant, and the same is true on the dusk flank after 3 h. When averaging the temperature, we neglect points at which the density is below 0.01 cm^{-3}. In fact, averaging temperatures over regions in which the density varies can be misleading, but generally speaking, it is clear that the dawn flank cools somewhat in our simulations while the dusk flank temperature remains relatively constant.

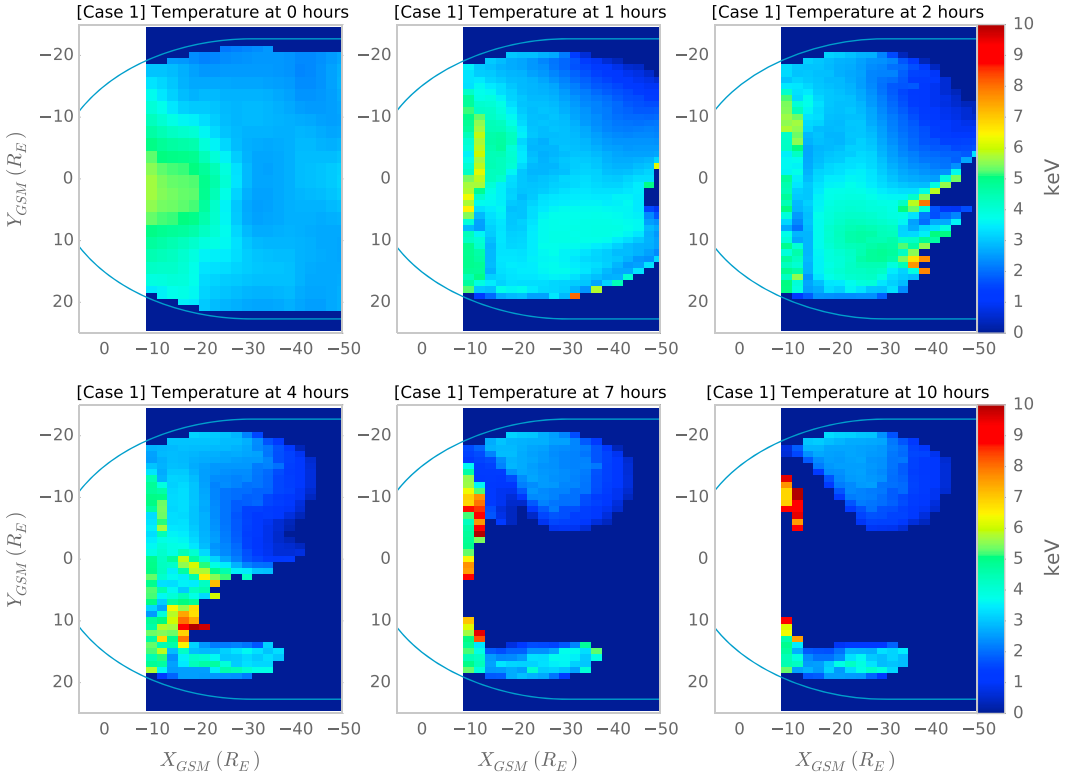

Figure 5. The hot component temperature from the Case 1 simulation is shown at times 0, 1, 2, 4, 7, and 10 h. The location of the magnetopause in the T01 magnetic field model is shown for reference. The hot plasma on in the duskside tail region at late times is due to the gradient drifting of energetic protons around a shallow B_Z minimum; their particle fluxes are low, and it is only due to the complete absence of cold particles in this region (given the artificial boundary condition) that the temperature appears so high.

3.2. Case 2

In case 2 we impose entry of new hot component plasma into an empty modeling region. We set the initial density to be zero. But as hot component plasma enters from the boundary, the density gradually increases along both flanks and within the premidnight sector and remains constant for the remainder of the simulation. We thus clearly see the entry of new plasma into the modeling region coming from our boundary condition, which we set based on the observed hot component plasma during NIMF intervals. It should also be noted that the hot component plasma in the THEMIS NIMF dataset likely originated during SIMF intervals, and the assumption that its entry into our modeling region is constant in time is probably not reasonable. However, it would take an unrealistically large amount of data to provide a statistically significant estimate of how the distant tail's hot component plasma varies with the length of time the IMF has been northward.

Because the phase space densities are highest at lower energies, the ion number density is predominantly composed of the colder particles which approximately drift along equipotential contours. The entry of new plasma from the boundary (Figure 6) is therefore somewhat predictable based on the potential contours shown in Figure 2. Some studies [e.g., *Wang et al.*, 2010] indicate the importance of diffusive transport (which we do not simulate) in bringing the cold magnetosheath particles across the tail and into the midnight plasma sheet. The temperature plots (Figure 7) show a dispersive entry of the protons, where the first protons to enter the modeling region are the hottest ones followed by successively cooler particles. This explains the apparent stratification of temperature displayed in Figure 7. As time progresses in our simulation, we begin to see the full energy spectrum of the particles as the slower low-energy particles have finally $E \times B$ drifted in and filled most of the magnetosphere. The regions near the potential maximum and minimum on the dawn and dusk flanks are regions of hot tenuous plasma because only hot particles can cross equipotentials and access these regions. In this run the dusk flank, which we define as $y > 15\,R_E$ and $-50\,R_E < x < -15\,R_E$, warms steadily from about 2.5 keV at $t = 1$ h to $\sim$ 4.3 keV at $t = 10$ h, and the dawn

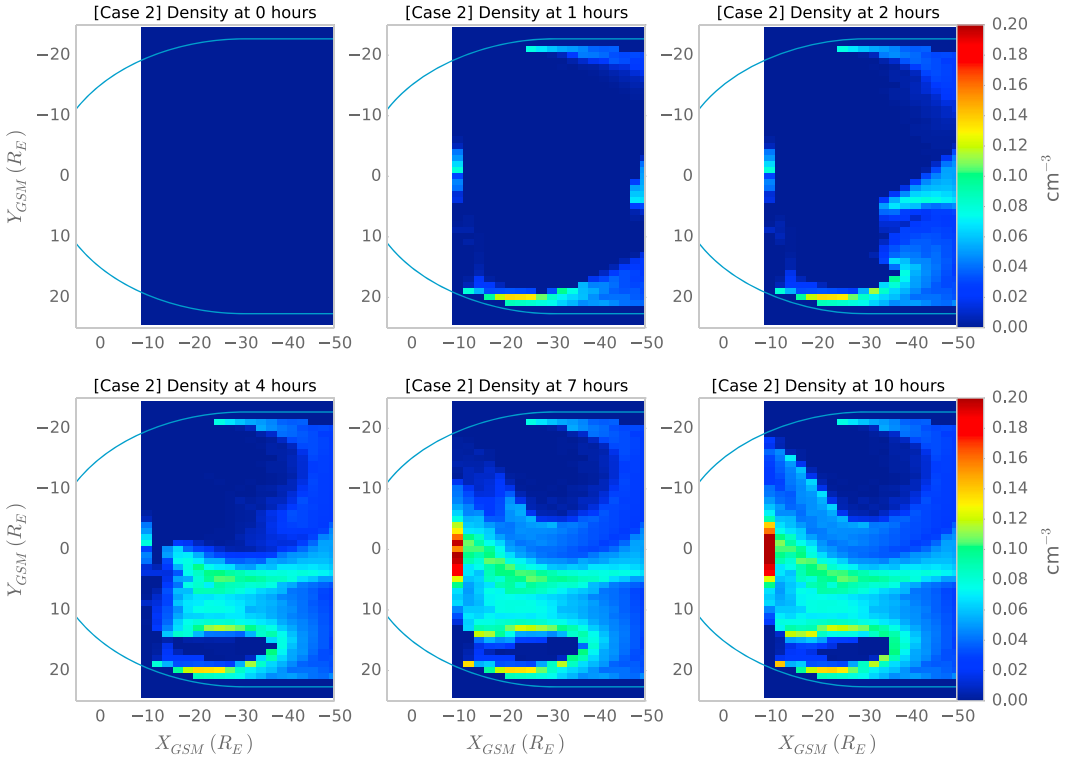

Figure 6. The hot component density from the Case 2 simulation is shown at times 0, 1, 2, 4, 7, and 10 h. The location of the magnetopause in the T01 magnetic field model is shown for reference.

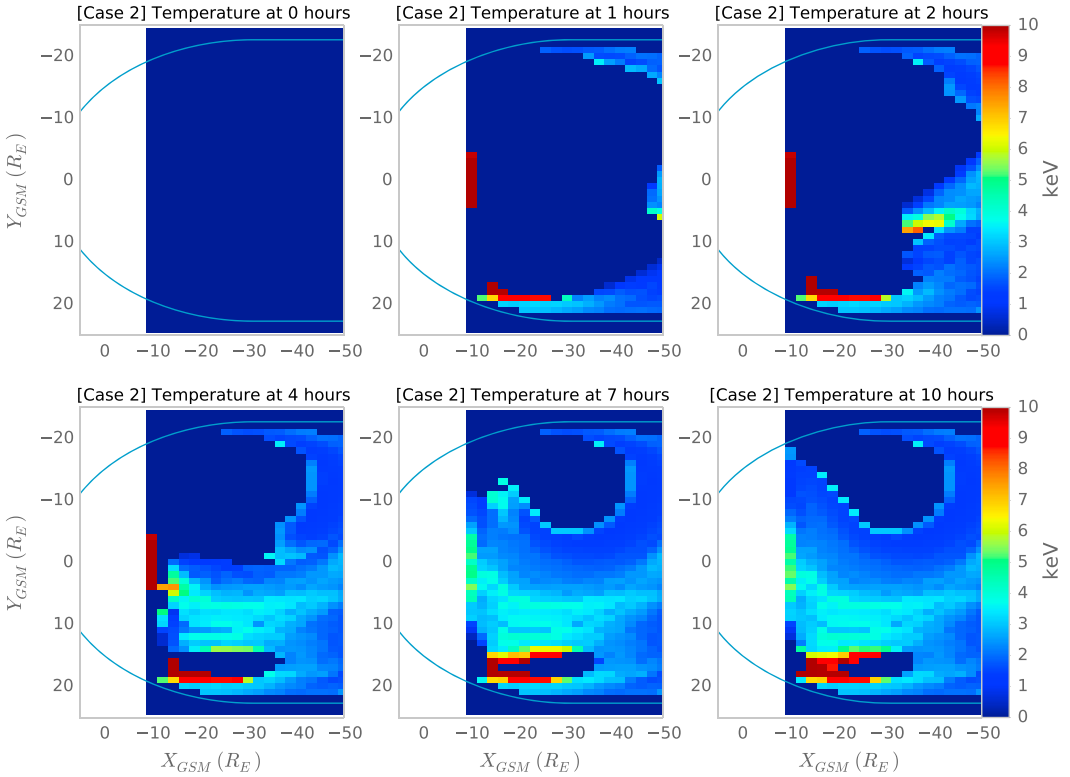

Figure 7. The hot component temperature from the Case 2 simulation is shown at times 0, 1, 2, 4, 7, and 10 h. The location of the magnetopause in the T01 magnetic field model is shown for reference.

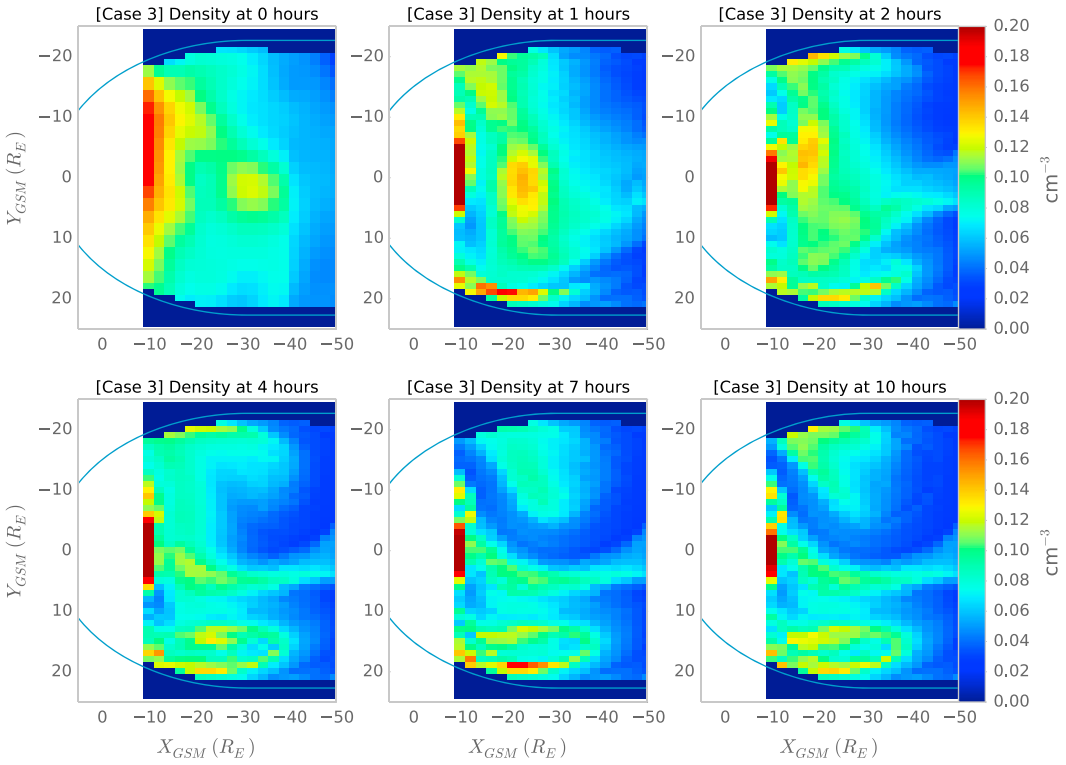

Figure 8. The hot component density from the Case 3 simulation is shown at times 0, 1, 2, 4, 7, and 10 h. The location of the magnetopause in the T01 magnetic field model is shown for reference.

flank temperature remains fairly steady at about 1.7 keV after $t = 2$ h. As before, we do not include points where the density is below 0.01 cm^{-3} in our averages.

3.3. Case 3

Case 3 is the sum of the previous two cases, where we simulate new, hot plasma entry in addition to the circulation of the preexisting hot component plasma. At $t = 0$ we are assuming that the IMF has recently turned northward, leaving the plasma sheet in a state typical of SIMF conditions. As in Case 2, we specify the boundary condition to use only the hot component phase space densities at the boundary consistent based on our NIMF THEMIS data. There is a slight decrease in the density from the initial condition to $t = 1$ hour but then the density evolution is seen to stay relatively constant throughout the simulation. This is the same trend observed in the [*Wing et al.*, 2005] study. Therefore, in the long run, the loss of the hotter ions is balanced by new influx of cold NIMF plasma sheet particles originating from the region farther down the tail and along the flanks.

Because of the inherent duskward gradient drift of the hotter particles, as time progresses in our simulations the dawn flank cools while the dusk flank either gets warmer or stays relatively constant. In this simulation run, which is arguably the closest approximation to what happens in the real magnetosphere in terms of initial and boundary conditions, the dusk flank temperature remains roughly the same throughout the simulation, while the dawn flank cools by about 15% from $t = 0$ to $t = 1$ h and then remains relatively constant. When comparing Figures 4, 6, and 8, it is seen that since density is dominated by the lower-energy ions whose drift paths closely follow equipotential contours, most of the hot component density along the flanks is actually coming from our initial condition (as is made clear in Figure 4) and circulates on closed drift paths (compare to Figure 2). Comparing Figures 5, 7, and 9, on the other hand, demonstrates that because hot ions are able to cross equipotential contours, the hot ions coming from the distant tail can contribute to the temperature in the region of plasma circulation along the flanks. There is a more noticeable contribution of the hot plasma from the distant tail to the dusk flank temperature than to the dawn flank temperature (compare, for example, Figures 5 and 9). This, of course, is to be expected since gradient drift drives hot plasma preferentially duskward. Figure 10 summarizes the evolution of density and temperatures on the dawn and dusk flanks from our simulations. Gradient drift can seemingly cool the hot component ions of the plasma

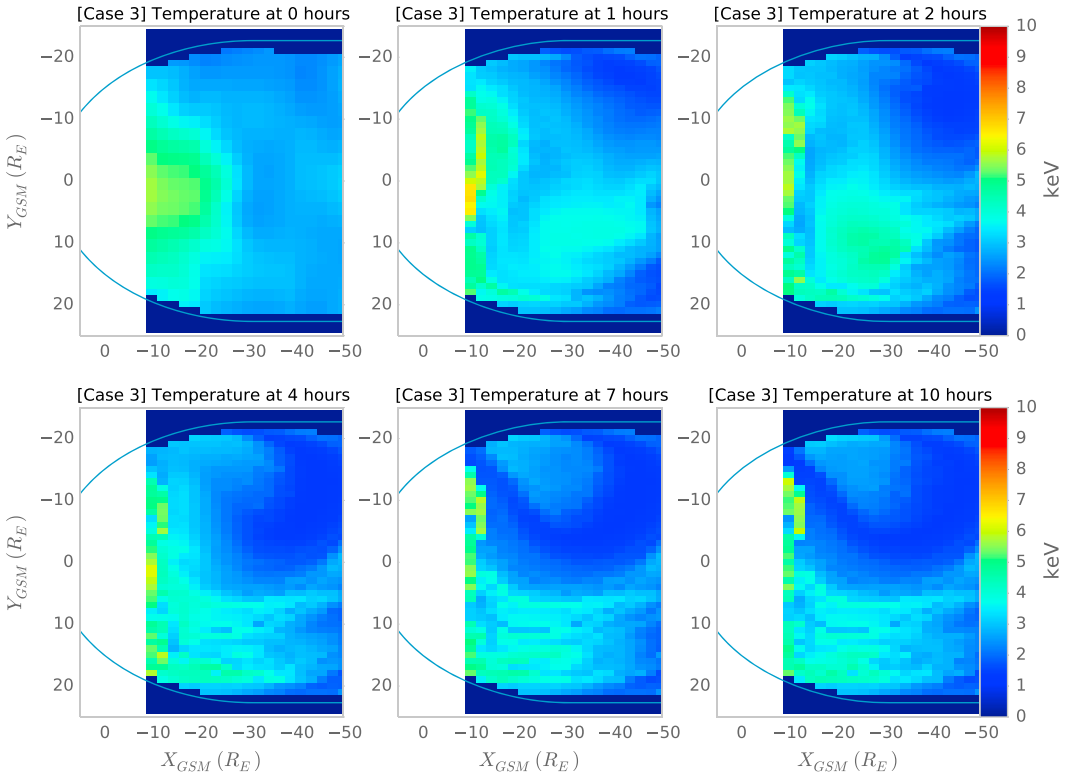

Figure 9. The hot component temperature from the Case 3 simulation is shown at times 0, 1, 2, 4, 7, and 10 h. The location of the magnetopause in the T01 magnetic field model is shown for reference.

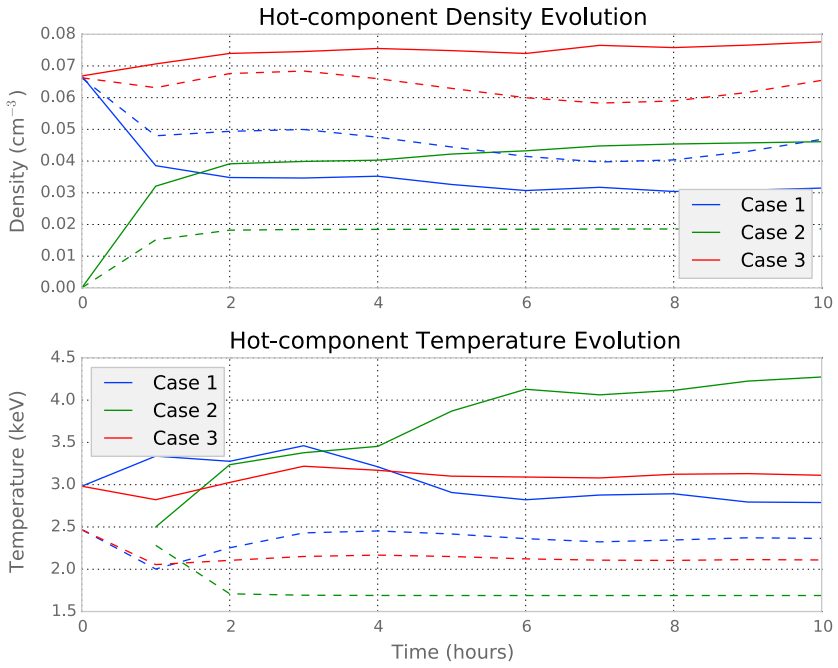

Figure 10. The evolution of (top) hot component density and (bottom) temperature on the dawn flank (solid lines) and dusk flank (dashed lines) is shown for each of the three cases simulated. Case 1 (blue curves) corresponds to Figures 4 and 5. Case 2 (green curves) corresponds to Figures 6 and 7. And Case 3 (red curves) corresponds to Figures 8 and 9. This figure (especially curves for Cases 1 and 3) can be compared with Figure 1c and 1d, which show similar curves obtained from a statistical analysis of observational data by *Wing et al.* [2005].

sheet on the dawn flank but not on the dusk flank. Again, we caution that in reality, the phase space density of hot component plasma in the distant tail is not likely to be constant during NIMF intervals. Most likely, it would decrease with time the longer the IMF is northward. As such, our closest approximation to reality may be a scenario that is somewhere between cases 1 and 3, even though this is somewhat speculative.

4. Discussion

4.1. Time-Independent Electric and Magnetic Field

There are several caveats when comparing the data in this study to the data in the [*Wing et al.*, 2005] study. First of all, this study produces a deterministic simulation with one specific time-independent magnetic and electric field, while *Wing et al.* [2005] look at observational data from numerous different events, in which the magnetic and electric fields could have been somewhat different for the different events. *Wing et al.* [2005] map the ionospheric DMSP data to the equatorial magnetosphere using the T96 magnetic field model. There are inherent uncertainties in the mapping, particularly in the x direction, which stem from the differences between the actual and T96 magnetic field at the time of the DMSP observations. In this paper, we impose a field model and examine how the particles evolve within this field. Since the THEMIS data set is equatorial and we focus on 90° pitch angles, we directly model equatorial plasma transport and avoid introducing any additional mapping errors that must be considered when comparing our results with those of *Wing et al.* [2005].

In this study, the magnetic field remains constant for up to 10 h, while in reality the magnetic field could have stayed northward for 10 continuous hours but its value would not have been constant. Because we impose a steady and time-independent magnetic and electric field, this study ignores certain mechanisms that normally operate in the real magnetosphere, such as diffusive transport and wave-particle interactions. The exclusion of these processes not only simplifies the model but also makes it easier to see the role that gradient drift plays in cooling the hot component ions of the plasma sheet during extended NIMF intervals.

4.2. DMSP Data

The *Wing et al.* [2005] study used DMSP data from 1992. Because 1992 is near solar maximum, their data has some inherent biases to those plasma sheet parameters that have solar cycle dependences, such as the solar wind and plasma sheet density which are both higher near solar maximum [*Borovsky et al.*, 1998; *Papitashvili et al.*, 2000]. Furthermore, because the DMSP detector was pointed upward and had limited pitch angle resolution, their data consists entirely of highly field-aligned precipitating particles. The DMSP satellites would not have observed the particles in our study since the particles in our study are confined to the equatorial plane. However, there is sufficient pitch angle scattering in the plasma sheet to at least partially isotropize the distribution so that the phase space densities of particles with 90° pitch angles should be close to that of precipitating particles. We did not calculate drift in the Wolf adiabatic approximation for bounce-averaged isotropic particles because the particle tracing code we developed will ultimately include drift across the magnetopause, for which the Wolf approximation is inappropriate.

Note that we specify an energy range for our particles, 32 eV–30 keV, that is similar to that of the DMSP data [e.g., *Wing et al.*, 2005]. Although this energy range overlaps the cold component ions, our phase space densities are specified only for the hot component ions.

4.3. Distribution Functions

The method used for inferring the plasma sheet properties from ionospheric observations by [*Wing et al.*, 2005] requires good ionosphere-magnetosphere mapping and is described in greater detail in their paper [*Wing et al.*, 2005]. They exclude electron acceleration events from their data as such events would distort the plasma sheet particle spectra and the remaining events are fitted to three spectral forms: (1) one-component Maxwellian, (2) two-component Maxwellian, and (3) kappa distribution. A one-component Maxwellian is used when the ion distribution has minimal separation in temperature, and the kappa distribution is used when the ion distribution contains a high-energy tail.

By fitting the differential energy flux to one of the aforementioned spectral forms, *Wing et al.* [2005] are able to take into account (via extrapolation) ions outside the DMSP detector's energy range (32 eV to 30 keV), and thus, their densities and temperatures are slightly higher than what they would have otherwise obtained. We use the energy range we model, not fitting it to a distribution function. However, our energy range is fairly comprehensive, so we do not believe this causes significant differences.

5. Summary

We investigated whether gradient drift can explain the cooling of the hot component ions of the plasma sheet during an extended NIMF interval. We traced the guiding center particle drift of equatorially mirroring protons in the T01 magnetic field and in the Weimer 2000 electric potential. We then mapped the resulting phase space distributions to realistic distributions based on THEMIS observations. Although our simulation results do not show cooling on the duskside of the magnetosphere due to gradient drift, we found that gradient drift can likely cool plasma sheet ions on the dawnside of the magnetosphere. The conclusion is the same even in under the assumption that the inflow of new hot component plasma from the distant tail is completely shut off. During extended intervals of NIMF, gradient drift could account for most of the cooling of the dawnside plasma sheet ions that was inferred by the statistical study of *Wing et al.* [2005] but is probably not sufficient to explain the cooling of the duskside plasma sheet ions. Other mechanisms, such as wave-mediated interactions between cold component and hot component ions or the more rapid loss of hotter ions to ionospheric precipitation may be necessary to fully explain the apparent cooling phenomenon.

Acknowledgments

The research at UCLA was supported by NSF GEM grant AGS-1003876, and the research at The Aerospace Corporation was supported by NSF GEM grant AGS-1003874. We thank Simon Wing of the Johns Hopkins Applied Physics Laboratory for his helpful discussions about this work. Simulation data used in this paper may be obtained by contacting the corresponding author, Colby Lemon.

Michael Liemohn thanks the reviewers for their assistance in evaluating this paper.

References

Baumjohann, W., and R. A. Treumann (1997), *Basic Space Plasma Physics*, p. 120, Imperial College Press, London, U. K.

Baumjohann, W., G. Paschmann, and C. A. Cattell (1989), Average plasma properties in the central plasma sheet, *J. Geophys. Res.*, *94*, 6597–6606.

Borovsky, J. E., and J. T. Steinberg (2006), The "calm before the storm" in CIR/magnetosphere interactions: Occurrence statistics, solar wind statistics, and magnetospheric preconditioning, *J. Geophys. Res.*, *111*, A07S10, doi:10.1029/2005JA011397.

Borovsky, J. E., M. F. Thomsen, and R. C. Elphic (1998), The driving of the plasma sheet by the solar wind, *J. Geophys. Res.*, *103*, 17,617–17,639.

Feldstein, Y. I., and Y. I. Galperin (1985), The auroral luminosity structure in the high-latitude upper atmosphere: Its dynamics and relationship to the large-scale structure of the Earth's magnetosphere, *Rev. Geophys.*, *23*, 217–275.

Fujimoto, M., T. Terasawa, T. Mukai, Y. Saito, T. Yamamoto, and S. Kokubun (1998), Plasma entry from the flanks of the near-Earth magnetotail: Geotail observations, *J. Geophys. Res.*, *103*(A3), 4391–4408, doi:10.1029/97JA03340.

Fujimoto, M., T. Mukai, A. Matsuoka, Y. Saito, H. Hayakawa, S. Kokubun, and R. P. Lepping (2000), Multi-point observations of cold-dense plasma sheet and its relation with tail-LLBL, *Adv. Space Res.*, *25*, 1607–1616, doi:10.1016/S0273-1177(99)00674-2.

Harel, M., R. A. Wolf, R. W. Spiro, P. H. Reiff, C.-K. Chen, W. R. Burke, F. J. Rich, and M. Smiddy (1981), Quantitative simulation of a magnetospheric substorm. 2: Comparison with observations, *J. Geophys. Res.*, *86*(A4), 2242–2260, doi:10.1029/JA086iA04p02242.

Hones, E. W. (1984), Plasma sheet behavior during substorms, in *Magnetic Reconnection in Space and Laboratory Plasmas*, edited by E. W. Hones, 178 pp., *Geophys. Monogr. Ser.* vol., 30, pp. 178–184, AGU, Washington, D. C.

Huang, C. Y., and L. A. Frank (1994), A statistical survey of the central plasma sheet, *J. Geophys. Res.*, *99*, 83–95, doi:10.1029/93JA01894.

Jordanova, V. K., J. U. Kozyra, G. V. Khazanov, A. F. Nagy, C. E. Rasmussen, and M. C. Fok (1994), A bounce-averaged kinetic model of the ring current ion population, *Geophys. Res. Lett.*, *21*, 2785–2788.

Kamide, Y., and J. A. Slavin (Eds.) (1986), *Solar Wind-Magnetosphere Coupling*, Terra Sci., Tokyo, Japan.

Kivelson, M. G., and C. T. Russell (1995), *Introduction to Space Physics*, p. 291–292, Cambridge Univ. Press, New York.

Lavraud, B., and V. K. Jordanova (2007), Modeling the effects of cold-dense and hot-tenuous plasma sheet on proton ring current energy and peak location, *Geophys. Res. Lett.*, *34*, L02102, doi:10.1029/2006GL027566.

Lavraud, B., M. F. Thomsen, J. E. Borovsky, M. H. Denton, and T. I. Pulkkinen (2006), Magnetosphere preconditioning under northward IMF: Evidence from the study of coronal mass ejection and corotating interaction region geoeffectiveness, *J. Geophys. Res.*, *111*, A09208, doi:10.1029/2005JA011566.

Lennartsson, W., and E. G. Shelley (1986), Survey of 0.1- to 16-keV/e plasma sheet ion composition, *J. Geophys. Res.*, *91*, 3061–3076.

Mauk, B. H., and C.-I. Meng (1991), The aurora and middle magnetospheric processes, in *Auroral Physics*, edited by C.-I. Meng et al., 223 pp., Cambridge Univ. Press, New York.

Maynard, N. C., E. A. Bielecki, and H. F. Burdick (1981), Instrumentation for vector electric field measurements from DE-B, *Space Sci. Instrum.*, *5*, 523–534.

Moldwin, M. B., and W. J. Hughes (1992), On the formation and evolution of plasmoids: A survey of ISEE 3 geotail data, *J. Geophys. Res.*, *97*(A12), 19,259–19,282, doi:10.1029/92JA01598.

Øieroset, M., J. Raeder, T. D. Phan, S. Wing, J. P. McFadden, W. Li, M. Fujimoto, H. Rème, and A. Balogh (2005), Global cooling and densification of the plasma sheet during an extended period of purely northward IMF on October 22–24, 2003, *Geophys. Res. Lett.*, *32*, L12S07, doi:10.1029/2004GL021523.

Papitashvili, V. O., N. E. Papitashvili, and J. H. King (2000), Solar cycle effects in planetary geomagnetic activity: Analysis of 36-year long OMNI dataset, *Geophys. Res. Lett.*, *27*, 2797–2800.

Prölss, G. W. (2004), *Physics of the Earth's Space Environment: An Introduction*, p. 270, Springer-Verlag, Berlin, Heidelberg, Germany.

Spence, H. E., and M. G. Kivelson (1993), Contributions of the low-latitude boundary layer to the finite width magnetotail convection model, *J. Geophys. Res.*, *98*(A9), 15,487–15,496, doi:10.1029/93JA01531.

Terasawa, T., et al. (1997), Solar wind control of density and temperature in the near-Earth plasma sheet: WIND/Geotail collaboration, *Geophys. Res. Lett.*, *24*, 935–938.

Thomsen, M. F., J. E. Borovsky, R. M. Skoug, and C. W. Smith (2003), Delivery of cold, dense plasma sheet material into the near-Earth region, *J. Geophys. Res.*, *108*(A4), 1151, doi:10.1029/2002JA009544.

Tsyganenko, N. A. (1989), A magnetospheric magnetic field model with a warped tail current sheet, *Planet. Space Sci.*, *37*, 5–20.

Tsyganenko, N. A. (2002a), A model of the near magnetosphere with a dawn-dusk asymmetry: 1. Mathematical structure, *J. Geophys. Res.*, *107*(A8), 1179, doi:10.1029/2001JA000219.

Tsyganenko, N. A. (2002b), A model of the near magnetosphere with a dawn-dusk asymmetry: 2. Parameterization and fitting to observations, *J. Geophys. Res.*, *107*(A8), 1176, doi:10.1029/2001JA000220.

Wang, C.-P., L. R. Lyons, M. W. Chen, and R. A. Wolf (2001), Modeling the quiet time inner plasma sheet protons, *J. Geophys. Res.*, *106*(A4), 6161–6178, doi:10.1029/2000JA000377.

Wang, C.-P., L. R. Lyons, T. Nagai, J. M. Weygand, and R. W. McEntire (2007), Sources, transport, and distributions of plasma sheet ions and electrons and dependences on interplanetary parameters under northward interplanetary magnetic field, *J. Geophys. Res.*, *112*, A10224, doi:10.1029/2007JA012522.

Wang, C.-P., L. R. Lyons, T. Nagai, J. M. Weygand, and A. T. Y. Lui (2010), Evolution of plasma sheet particle content under different interplanetary magnetic field conditions, *J. Geophys. Res.*, *115*, A06210, doi:10.1029/2009JA015028.

Wang, C.-P., M. Gkioulidou, L. R. Lyons, and V. Angelopoulos (2012), Spatial distributions of the ion to electron temperature ratio in the magnetosheath and plasma sheet, *J. Geophys. Res.*, *117*, A08215, doi:10.1029/2012JA017658.

Weimer, D. R. (2001), An improved model of ionospheric electric potentials including substorm perturbations and application to the Geospace Environment Modeling November 24, 1996, event, *J. Geophys. Res.*, *106*(A1), 407–416, doi:10.1029/2000JA000604.

Weiss, L. A., P. H. Reiff, J. J. Moses, R. A. Heelis, and B. D. Moore (1992), Energy dissipation in substorms, in *Proceeding of the International Conference on Substorms (ICS- 1)*, 309 pp., Eur. Space Agency Spec. Publ., ESA SP-335, Paris, France.

Wing, S., and P. T. Newell (1998), Central plasma sheet ion properties as inferred from ionospheric observations, *J. Geophys. Res.*, *103*(A4), 6785–6800, doi:10.1029/97JA02994.

Wing, S., and P. T. Newell (2002), 2D plasma sheet ion density and temperature profiles for northward and southward IMF, *Geophys. Res. Lett.*, *29*(9), 1307, doi:10.1029/2001GL013950.

Wing, S., J. R. Johnson, P. T. Newell, and C.-I. Meng (2005), Dawn-dusk asymmetries, ion spectra, and sources in the northward interplanetary magnetic field plasma sheet, *J. Geophys. Res.*, *110*, A08205, doi:10.1029/2005JA011086.

Young, S. L., R. E. Denton, B. J. Anderson, and M. K. Hudson (2008), Magnetic field line curvature induced pitch angle diffusion in the inner magnetosphere, *J. Geophys. Res.*, *113*, A03210, doi:10.1029/2006JA012133.